NJC

Accepted Manuscript

This is an *Accepted Manuscript*, which has been through the Royal Society of Chemistry peer review process and has been accepted for publication.

Accepted Manuscripts are published online shortly after acceptance, before technical editing, formatting and proof reading. Using this free service, authors can make their results available to the community, in citable form, before we publish the edited article. We will replace this *Accepted Manuscript* with the edited and formatted *Advance Article* as soon as it is available.

You can find more information about *Accepted Manuscripts* in the Information for Authors.

Please note that technical editing may introduce minor changes to the text and/or graphics, which may alter content. The journal's standard Terms & Conditions and the Ethical guidelines still apply. In no event shall the Royal Society of Chemistry be held responsible for any errors or omissions in this *Accepted Manuscript* or any consequences arising from the use of any information it contains.

ROYAL SOCIETY OF CHEMISTRY

www.rsc.org/njc

Journal Name

ARTICLE

A novel dual-functional fluorescent chemosensor for selective detection of 2,4,6-trinitrotoluene and Hg^{2+}

Received 00th January 20xx,
Accepted 00th January 20xx

DOI: 10.1039/x0xx00000x

www.rsc.org/

MeiMei Liu, Gang Li * and ZhuHong Cheng

Herein we develop a dual-functional fluorescent chemosensor R/Au/Tb-BTC. This chemosensor was prepared by immobilizing rhodamine derivative probes (R) onto the surface of metal-organic framework Tb-BTC via Au nanoparticles (Au NPs). The chemosensor was characterized by X-ray powder diffraction (XRD), scanning electron microscopy (SEM), fourier transform infrared spectroscopy (FT-IR) and UV-vis spectrum. R/Au/Tb-BTC was applied in detection of nitroaromatic compounds and Hg^{2+}, which were detected by the Tb-BTC and the R respectively. Nitroaromatic compounds, such as 2,4,6-trinitrotoluene (TNT), nitrobenzene (NB) and 4-Nitrophenol (PNP), could reduce the fluorescence intensity of the R/Au/Tb-BTC in ethanol solution. Thus the R/Au/Tb-BTC can selectively and sensitively detect nitroaromatic compounds, especially TNT. Meanwhile, R/Au/Tb-BTC has both fluorescence and colorimetry performance for detection of Hg^{2+} in aqueous solution. It presents excellent anti-disturbance ability when exposed to a series of competitive cations such as Na^+, K^+, Ag^+, Li^+, Ba^{2+}, Ca^{2+}, Pb^{2+}, Cd^{2+}, Co^{2+}, Cu^{2+}, Mg^{2+}, Mn^{2+}, Ni^{2+}, and Zn^{2+}. More importantly, when TNT and Hg^{2+} coexist in ethanol solution, the two pollutants can be detected using one chemosensor R/Au/Tb-BTC.

1 Introduction

The nitroaromatic compounds, such as 2,4,6-trinitrotoluene (TNT), nitrobenzene (NB) and 4-Nitrophenol (PNP), are toxic pollutants, especially TNT. TNT is the most well-known explosive and commonly used for military application. So the selective and sensitive detection of nitroaromatic compounds is of great current interest both in national security and environmental protection. Some new approaches for detecting nitroaromatic compounds have been developed, such as fluorescent chemosensor method.[1] Compared to other traditional methods like gas chromatography,[2] ion mobility spectrometers,[3] mass spectrometry,[4] Raman spectroscopy,[5] neutron analysis[6] and X-ray detection,[7] fluorescent chemosensor method is more economic and portable. Consequently, it seems to be very promising to rapidly and real-time detect nitroaromatic compounds using a chemosensor.[8]

Metal-organic frameworks (MOFs), a fantastic type of porous crystalline solid constructed from the limitless choice of metals and organic bridging ligands, have gained significant interests during the past decade, owing to their intriguing variety of architectures, topologies and their many attractive applications in hydrogen storage,[9] gas separation,[10] heterogeneous catalysis,[11] photonics[12] and sensing.[13] Very recently, lanthanide-based MOFs (Ln-MOFs) have attracted much attention in the aspect of luminescent sensing, which was due to their exceptional optical properties arising from their 4f electrons.[14] Several lanthanide-derived MOFs for the detection of nitroaromatic compounds have been reported. Qiu et al. reported the syntheses of lanthanide MOF $[Eu(BDC)_3(H_2O)_2]_n$ nanorods,[15] which were applied to detect nitroaromatic explosives. Xu et al. synthesized luminescent lanthanide-based MOF $Eu_2(BDC)_3(H_2O)_2 \cdot (H_2O)_2$ and demonstrated its selective luminescent sensing of nitroaromatic explosives.[16] Xiao et al. reported the syntheses of nanoscale terbium-based MOF $[Tb(1,3,5\text{-}BTC)]_n$ and demonstrated its application in luminescent sensing of picric acid (PA).[17] The magnetic MOF nanospheres Fe_3O_4@Tb-BTC that exhibited high sensitivity for sensing 2,4,6-trinitrotoluene were successfully designed by Qian et al.[18]

Mercury ion is a highly dangerous heavy metal ion and can be easily converted into the most toxic form like methyl mercury by bacteria. It is widely distributed in the environment due to the various human activities. When Hg^{2+} subsequently bioaccumulates through the food chain, it can damage the brain, heart, kidney, nervous system and endocrine system of humans and animals.[19] Therefore, the rapid and sensitive detection of Hg^{2+} in the environment is of great importance to environmental science. It is well-known that fluorescence method is a particularly suitable method for monitoring low-level Hg^{2+} due to its sensitivity, facility and rapidness.[20] Compared to fluorescence-based molecular probes,[21] fluorescence-based chemosensors increase the hydrophilicity, as well as avoid the self-quenching of probe

State Key Laboratory of Fine Chemicals, School of Chemical Engineering, Dalian University of Technology, Dalian, 116024, P. R. China.
E-mail: liganghg@dlut.edu.cn;
Fax: +86-411-8498-6113; Tel: +86-411-8498-6113
† Electronic Supplementary Information (ESI) available. See DOI: 10.1039/x0xx00000x

molecules.[22] In our previous work, two fluorescent chemosensors Au-HMS-probe and HMS-Ag-R were prepared by immobilizing rhodamine derivative probes onto the surface of hexagonal mesoporous silica (HMS) via noble metal nanoparticles (Au NPs or Ag NPs) as connectors. Both of them achieved excellent sensitivity and selectivity for detection of Hg^{2+} in aqueous media.[23] However, all these chemosensors can only detect a single substance.

There are few papers about detecting two different kinds of pollutants in environment with one fluorescent chemosensor. Herein, we combined the metal organic frameworks Tb-BTC with the rhodamine derivative probes (R) via Au nanoparticles (Au NPs) and prepared a dual-functional fluorescent chemosensor R/Au/Tb-BTC for detecting nitroaromatic compounds and Hg^{2+}. The Au NPs on the Tb-BTC was prepared through glucose reduction and could immobilize the R via Au-N bond. The chemosensor R/Au/Tb-BTC was successfully endowed with dual functionality, which showed high sensitivity and selectivity for the luminescent sensing of nitroaromatic compounds, especially TNT, in ethanol solution, and also exhibited excellent performance for detection of Hg^{2+} in aqueous solution. Moreover, when TNT and Hg^{2+} coexist in ethanol solution, the R/Au/Tb-BTC could detect them respectively using different excitation wavelengths.

2 Experimental

2.1 Reagents

Terbium(Ⅲ) nitrate hydrate ($Tb(NO_3)_3•6H_2O$) was purchased from energy chemical Reagent Co., Ltd. 1,3,5-Benzenetricarboxylic acid (H_3BTC), rhodamine B (RhB) and tris(2-aminoethyl)amine were obtained from J&K. Anhydrous sodium acetate (CH_3COONa), anhydrous sodium sulphate (Na_2SO_4), dichloromethane, methanol and toluene were purchased from Tianjin Kemiou Chemical Reagent Co., Ltd. 2,4,6-trinitrotoluene (TNT) (dissolved in methanol solution) was purchased from Aladdin reagent company. $HAuCl_4•4H_2O$ was purchased from Shanghai Chemical Reagent Co., Ltd. All chemicals were of AR grade and used as received.

2.2 Characterization

X-Ray diffraction (XRD) patterns were obtained at room temperature on a Rigaku D/MAX-2400 X-ray powder diffraction (Japan) using Cu Kα radiation, operating at 40 kV and 100 mA. Scanning electron microscopy (SEM) images were obtained on a HITACHI FE-SEM S-4800 scanning electron microscopy. FT-IR spectra were recorded on a Bruker EQUINOX 55 spectrometer, using the KBr pellet technique. UV-vis spectra were measured on a Jasco UV-550 spectrophotometer. The photoluminescence (PL) spectra were taken on a Hitachi F-7000 fluorescence spectrophotometer at room temperature. Spectra in solid-state were recorded with excitation and emission slit widths of 2.5 nm, 600 V of voltage; spectra in suspension solution were recorded with excitation and emission slit widths of 5 nm, 700 V of the voltage.

2.3 Synthesis of Tb-BTC

In a typical solvothermal synthesis, $Tb(NO_3)_3•6H_2O$ (127 mg, 0.28 mmol), 1,3,5-H_3BTC (20 mg, 0.1 mmol) and CH_3COONa (16 mg, 0.2 mmol) were dissolved in co-solvents of DMF (4 mL), ethanol (4 mL) and H_2O (3.2 mL) at room temperature. A white suspension was obtained after further stiring for 30 min in a solvothermal vessel. The vessel was sealed and heated to 80℃ at a rate of 2℃/min for 24 h. The product was collected by centrifugation, washed several times with ethanol and dried overnight at 60℃.

2.4 Preparation of Au/Tb-BTC

Typically, Au/Tb-BTC was prepared by glucose reduction method. Firstly, 1.05×10^{-2} g $HAuCl_4•4H_2O$ was dissolved in 50 mL of deionized water. Then 1 g prepared Tb-BTC sample and 0.35 g glucose were added. The mixture was heated to 368 K and stirred for 1 h. The collected powder was washed several times with deionized water. The Au/Tb-BTC composite was obtained after dried overnight at 60℃.

2.5 Synthesis of rhodamine derivative

The rhodamine derivative R was prepared by the method reported in the literature.[24] To a 100 mL flask, under nitrogen, 1 g rhodamine B and 5 mL tris(2-aminoethyl)amine were dissolved in 60 mL methanol and kept at 353 K for several hours until the solution color turned to yellow from pink. After cooling to room temperature, the solvent was evaporated in vacuo. CH_2Cl_2 (100 mL) and deionized water (200 mL) were added into the residue after evaporation and the organic layer was separated. The CH_2Cl_2 layer was washed several times with deionized water followed by drying with anhydrous Na_2SO_4 overnight. After filtration of sodium sulphate, a yellow oil denoted as R was obtained after evaporating the solvent in vacuo.

2.6 Preparation of R/Au/Tb-BTC chemosensor

Au/Tb-BTC (1 g) and R (0.57 g) were dissolved in anhydrous toluene (50 mL) and stirred for 48 h at ambient temperature. The collected powder was washed several times with toluene to remove excess R. R/Au/Tb-BTC chemosensor was obtained after dried. The detailed synthetic route of R/Au/Tb-BTC was illustrated in Scheme 1.

2.7 Fluorescence spectrometric titration experiments

For the sensing of TNT, 25 mg R/Au/Tb-BTC was dispersed in 50 mL of ethanol (0.5 mg mL^{-1}). Each time, 2.0 mL R/Au/Tb-BTC suspension was added to a quartz cuvette with 1 cm optical path length. The corresponding fluorescence emission spectra, which were excited at 353 nm, were recorded after injecting various amounts of TNT into the suspension of R/Au/Tb-BTC. The interference tests for other nitroaromatic compounds and some common organic chemicals were similar to the above. For the sensing of Hg^{2+} in aqueous solution, as well as the interference test for other metal ions, 25 mg R/Au/Tb-BTC was dispersed in 50 mL of deionized water (0.5 mg mL^{-1}). Corresponding fluorescence emission spectra excited at 530

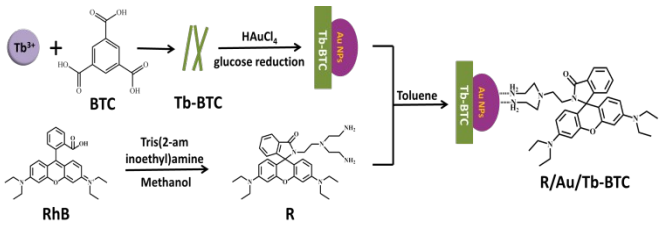

Scheme 1 Schematic illustration of the preparation of R/Au/Tb-BTC.

were monitored after injecting different amounts of metal ions into the quartz cuvette containing 2.0 mL R/Au/Tb-BTC aqueous suspension. For the sensing of both TNT and Hg^{2+} in ethanol solution, corresponding fluorescence emission spectra were monitored after injecting different amounts of TNT and Hg^{2+} ions simultaneously into the quartz cuvette.

3 Results and discussion

3.1 Characteristics of R/Au/Tb-BTC chemosensor

A dual-functional fluorescent chemosensor R/Au/Tb-BTC for detecting nitroaromatic compounds and Hg^{2+} was established by immobilizing rhodamine derivative onto Tb-BTC via Au NPs. The metal organic frameworks Tb-BTC was prepared through a typical solvothermal synthetic method. The Au NPs on the Tb-BTC was prepared through glucose reduction and could immobilize the R via Au-N bond. The X-ray diffraction (XRD) patterns of Tb-BTC, Au/Tb-BTC and R/Au/Tb-BTC are given in Fig. 1. The XRD pattern of the synthesized Tb-BTC (Fig. 1a) is identical to Tb-MOF-76 reported in previous literature.[25] Compared with Tb-BTC, the diffraction peak position of Au/Tb-BTC (Fig. 1b) changes after the introduction of Au NPs with glucose reduction method. It means that the Tb-BTC transforms from the Tb-MOF-76 to a new phase during the reduction process of $HAuCl_4$. The crystal-to-crystal transformation may be due to reconstruction during $HAuCl_4$ reduction process with glucose. These diffraction peaks correspond with Tb-MOF which was prepared by Cai et al. with a green coordination modulation method with KCl.[26] For R/Au/Tb-BTC (Fig. 1b), the peaks are identical to those of Au/Tb-BTC. It suggests the introduction of R doesn't change the structure of Au/Tb-BTC. In addition, the characteristic peaks of Au NPs can be clearly observed in Fig. 1b. Both Au/Tb-BTC and R/Au/Tb-BTC samples present X-ray reflections at 2θ = 38.2°, 44.5°, 77.6°, which correspond to the (111), (200) and (311) planes of the Au NPs.

The SEM images of Tb-BTC, Au/Tb-BTC and R/Au/Tb-BTC are shown in Fig. 2. The Tb-BTC presents relatively uniform strip-like crystals with a length of 4-5 μm (Fig. 2a). However, the Au/Tb-BTC crystals change to homogeneous puzzle-like sheets with the jagged edges after the introduction of Au NPs (Fig. 2b). It suggests the morphology of Tb-BTC changes to a new form due to the reduction process of Au NPs. This result corresponds with that of XRD. Furthermore, the introduction of R doesn't change the sheet morphology of Au/Tb-BTC (Fig. 2c).

The FT-IR spectra of Tb-BTC, Au/Tb-BTC, R/Au/Tb-BTC and

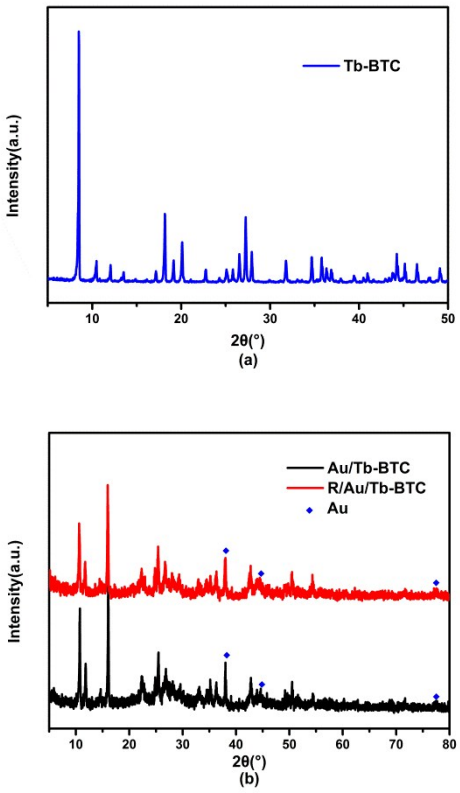

Fig. 1 X-ray diffraction patterns: (a) Tb-BTC; (b) Au/Tb-BTC and R/Au/Tb-BTC.

R are shown in Fig. 3. Samples Tb-BTC, Au/Tb-BTC, R/Au/Tb-BTC exhibit characteristic asymmetric stretching vibrations of carboxylate groups in the range of 1490-1590 cm^{-1} and the symmetric vibrations centered at 1380 cm^{-1}. Interestingly, new transmission bands 2970 and 2927 cm^{-1} are observed in the FT-IR spectrum of the R/ Au/Tb-BTC in comparison with the spectra of Tb-BTC and Au/Tb-BTC. These bands are assigned to the asymmetric and symmetric stretching vibrations of the methylene group (CH_2) in the alkyl chain. This feature also appears in the FT-IR spectrum of R, and there is no CH_2 in BTC, which suggests successful grafting of R onto the Au/Tb-BTC. Moreover, comparing with the spectra of Tb-BTC and Au/Tb-BTC, new band 1267 cm^{-1} which is assigned to the stretching vibration of the C-N in the R is also observed in the FT-IR spectra of the R/Au/Tb-BTC and R. This is another evidence for the successful immobilization of rhodamine derivative on the Au/Tb-BTC. In addition, in the spectrum of R + Au/Tb-BTC (Fig. S1, ESI†), which was the blend powder of R and Au/Tb-BTC, the characteristic stretching vibrations of carboxylate groups, methylene group (CH_2) and the C-N could also be observed.

The diffuse reflectance UV-vis spectra are used to confirm the existence of Au NPs and R (Fig. 4). Comparing with the spectrum of Tb-BTC, the spectrum of Au/Tb-BTC exhibits a significant peak centered at 535 nm which could be attributed to the Plasmon resonance absorbance of the Au NPs. This is another valid evidence that the Au NPs exist in the composite. Fig. 4 further shows that R anchors on the Au/Tb-BTC. A series of characteristic bands at 240, 280 and 320 nm emerge in the

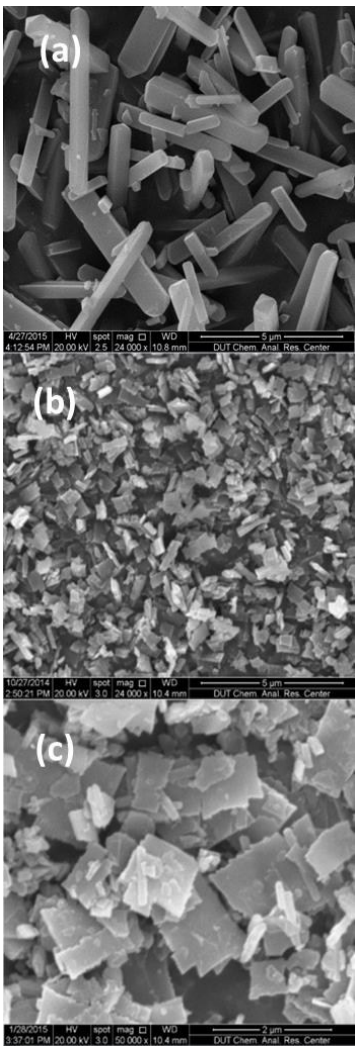

Fig.2 SEM images: (a) Tb-BTC; (b) Au/Tb-BTC; (c) R/Au/Tb-BTC.

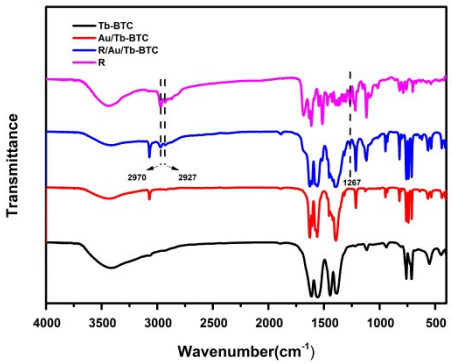

Fig.3 FT-IR spectra of Tb-BTC, Au/ Tb-BTC, R/ Au/ Tb-BTC and R.

spectra of both R and R/Au/Tb-BTC. These bands could be attributed to the typical electronic transition of the aromatic ring.[24] In addition, in the spectrum of R + Au/Tb-BTC (Fig. S2, ESI†), the characteristic bands of Au NPs and the aromatic ring could also be observed. But compared with R and R + Au/Tb-BTC, slight blue shifts for the intense absorption band at 280

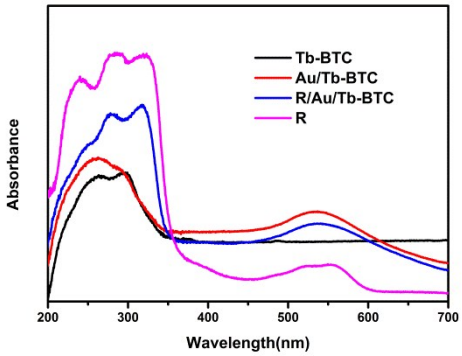

Fig.4 UV-vis spectra of Tb-BTC, Au/Tb-BTC, R/Au/Tb-BTC and R.

Table 1 Elemental analyses of Au/Tb-BTC and R/Au/Tb-BTC.

Sample	N (wt%)	C (wt%)
Au/Tb-BTC	0.08	27.12
R/Au/Tb-BTC	1.51	33.83

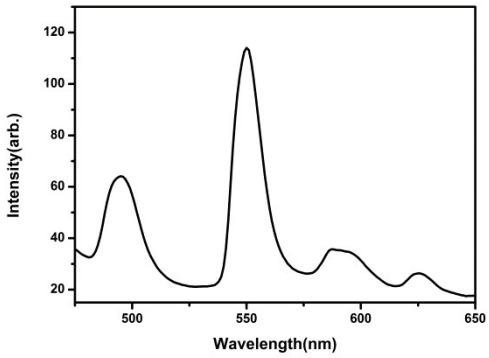

Fig.5 Solid-state PL emission spectrum of the R/Au/Tb-BTC (excited at 353 nm).

and 320 nm could be seen in the spectrum of R/Au/Tb-BTC, which implies the successful incorporation of R onto the surface of Au NPs and the R/Au/Tb-BTC is not a mixture of R and Au/Tb-BTC.

Elemental analysis (C and N) was also carried out to determine whether the rhodamine derivative was grafted onto the Au/Tb-BTC. The elemental analysis results of Au/Tb-BTC and R/Au/Tb-BTC were summarized in Table 1. As we can see, the Au/Tb-BTC contains 27.12 wt% of C which comes from the BTC. Compared with Au/Tb-BTC, mass percentage of C and N in R/Au/Tb-BTC increased about 6.71 wt% and 1.43 wt%, respectively. Accordingly, the increased mass ratio (C/N) in R/Au/Tb-BTC is 4.69. It is close to the theoretical ratio (C/N) 4.85 of R. This result gives another evidence for the successful immobilization of rhodamine derivative on the Au/Tb-BTC.

The solid-state R/Au/Tb-BTC displays strong luminescence at 493 nm, 550 nm, 584 nm and 625 nm upon excitation at 353 nm at room temperature (Fig. 5), and they are attributed to $^5D_4 \rightarrow {}^7F_3$, $^5D_4 \rightarrow {}^7F_4$, $^5D_4 \rightarrow {}^7F_5$ and $^5D_4 \rightarrow {}^7F_6$ transitions of Tb^{3+} ions, respectively. In addition, in the presence of Hg^{2+}, the

peak centered at 584 nm is also due to the opening-Spirolactam form of the rhodamine group.[22b] So in order to only get the fluorescence change in the event of the Hg^{2+} induced spirolactam ring opening in the following detection experiments, the luminescence of the R/Au/Tb-BTC at 584 nm is excited at 530 nm when only detecting Hg^{2+}, and in this way, there won't be the characteristic luminescence peaks of Tb^{3+} ions.[25b,27]

3.2 Luminescent sensing properties

The chemosensor R/Au/Tb-BTC connected the remarkable fluorescent Tb-BTC with the rhodamine derivative, thus this sensor has advantages of these two fluorescence probes. As previously reported, MOF-76 ($[Tb(1,3,5\text{-}BTC)]_n$) exhibits significant luminescence quenching effects for nitroaromatic compounds in ethanol solution.[16-18] The R exhibits high selectivity for Hg^{2+} in aqueous solution.[23] In this work, the R/Au/Tb-BTC was endowed with dual functionality, it means that the R/Au/Tb-BTC can not only detect nitroaromatic compounds using Tb-BTC, but also can recognize Hg^{2+} with the R. Fig. 6 showed the fluorescence changes of R/Au/Tb-BTC with increasing TNT in ethanol solution. As we can see, the strong luminescence quenching effects were observed for TNT. The luminescence quenching efficiency (LQE) was calculated by the equation LQE = $[(I_0\text{-}I)/I_0\times100\%]$, where I_0 was the initial fluorescence intensity of R/Au/Tb-BTC, I was the fluorescence intensity after adding different amount of TNT. The luminescence quenching efficiency exceeded 45 % when the concentration of TNT reached 1.85×10^{-6} M. Meanwhile, the green fluorescence of the solution faded under the 254 nm UV light (Fig. 6 inset). Whereas the quenched efficiencies of several other nitroaromatics such as NB, 4-Nitrophenol, were far less than that of TNT. Furthermore, some common organic chemicals, including PhMe, Nitromethane, benzene, THF and DMSO, showed almost no effects upon the luminescence of the R/Au/Tb-BTC, as can be seen from Fig. 7. The results obtained above clearly demonstrate an extremely high selectivity and sensitivity of the R/Au/Tb-BTC for detection of nitroaromatic compounds, especially TNT. This may be attributed to the fact that nitroaromatic compounds are good electron acceptors as substitution of the electron-withdrawing nitro groups on the aromatic ring lowers the energy of the empty π * orbitals, and the R/Au/Tb-BTC consists of Tb-BTC that can excite electrons to perform as excellent electron donors. These electrons can be transferred into the nitroaromatics. Luminescence quenching is achieved through an electron-transfer donor-acceptor methanism.[28] In addition, compared to other nitroaromatic compounds such as NB and PNP, TNT has a much higher quenching efficiency. It may be due to the lower LUMO level of TNT,[29] the excited electrons in the Tb-BTC could be more easily transferred into the TNT. Moreover, strong supramolecular interactions (e.g. hydrogen bonding) between the Tb-BTC and the TNT may also facilitate the charge transfer between them, therefore a much higher quenching efficiency of TNT is obtained.

An idealized mode for R/Au/Tb-BTC with Hg^{2+} was shown in Fig. 8. The interaction of the R on the surface of Au/Tb-BTC

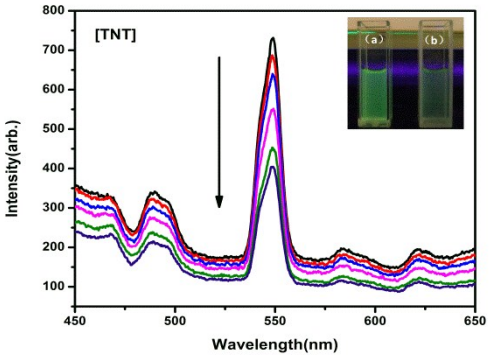

Fig.6 Emission spectra of R/Au/Tb-BTC with different concentration of TNT (0-1.85×10^{-6} M). The excitation wavelength is 353 nm. Inset: the fluorescence change (a) R/Au/Tb-BTC (b) R/Au/Tb-BTC + 1.85×10^{-6} M TNT.

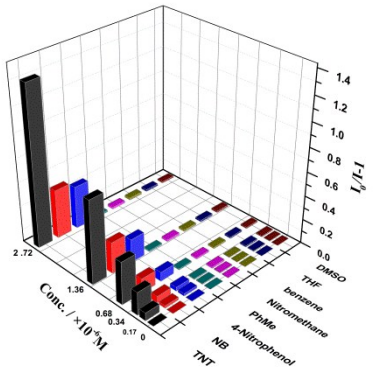

Fig.7 Fluorescence quenching results of nitroaromatic compounds and some commonly found interferents, including PhMe, Nitromethane, benzene, THF and DMSO, to the emission of the R/Au/Tb-BTC at various concentration in ethanol solution.

with Hg^{2+} induced a highly conjugated rhodamine system via formation of opened-spirolactam to give a strong fluorescence emission.[24]

The fluorescence spectra of R/Au/Tb-BTC with varying Hg^{2+} concentration in aqueous solution were shown in Fig. 9. Free R/Au/Tb-BTC suspension showed very weak fluorescence intensity at 584 nm (excited at 530 nm). Upon addition of Hg^{2+}, an enhancement of fluorescence intensity at 584 nm was observed, which was due to the opening-Spirolactam form of rhodamine groups induced by the complexation of R with the Hg^{2+}. At the same time, the color of the solution changed from white to pink and the solution showed an pink fluorescence change under the 365 nm UV light (Fig. 9 inset). In addition, we also investigated the fluorescence emission changes of R/Au/Tb-BTC with various biologically and environmentally relevant metal ions such as Na^+, K^+, Li^+, Ca^{2+}, Ba^{2+}, Pb^{2+}, Co^{2+}, Ag^+, Mg^{2+}, Mn^{2+},Zn^{2+}, Cd^{2+}, Ni^{2+} and Cu^{2+} (Fig. 10). Typically, 5×10^{-8} M of other competing metal ions were respectively added into the R/Au/Tb-BTC suspension, and the fluorescence enhancing results were recorded. Then, 5×10^{-8} M of Hg^{2+} was added to the former solution for another fluorescence measurement. It can be seen that the fluorescence intensities of R/Au/Tb-BTC

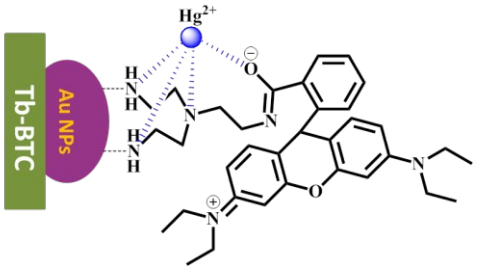

Fig.8 The coordination mode for R/Au/Tb-BTC with Hg^{2+}.

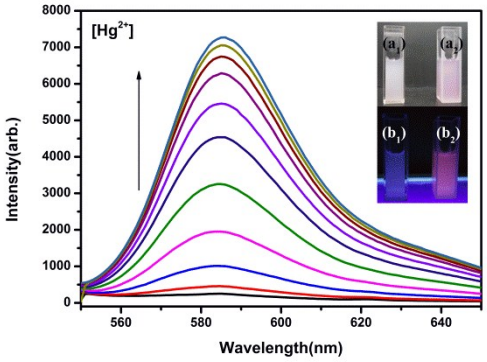

Fig.9 Fluorescence spectra of R/Au/Tb-BTC with different concentrations of Hg^{2+} (0-25×10^{-8} M) in aqueous solution when excited at 530 nm. Inset: the color change (a_1) R/Au/Tb-BTC (a_2) R/Au/Tb-BTC + 25×10^{-8} M Hg^{2+}; the fluorescence change (b_1) R/Au/Tb-BTC (b_2) R/Au/Tb-BTC + 25×10^{-8} M Hg^{2+}.

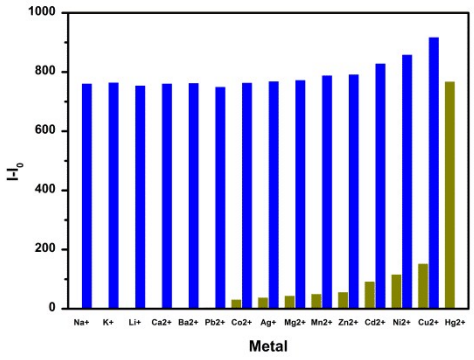

Fig.10 Relative fluorescence intensity ($I-I_0$) at 584 nm of R/Au/Tb-BTC to other metal ions and to Hg^{2+} (5×10^{-8} M, the olive green bar) or the mixture of other metal ions with Hg^{2+} (5×10^{-8} M, the blue bar).

showed no change or a slight change in the presence of the competitive metal ions. However an obvious fluorescence response was induced after adding Hg^{2+}, which indicated that the R/Au/Tb-BTC had a good selectivity for Hg^{2+}. The special selectivity was probably due to the following factors: the suitable coordination geometry conformation of the receptor, the larger radius of the Hg^{2+}, the nitrogen-affinity and the amide deprotonation ability of the Hg^{2+}.[30]

The detection property of the R/Au/Tb-BTC for TNT was further investigated in the presence of Hg^{2+} in ethanol solution. As shown in Fig. 11, free R/Au/Tb-BTC solution showed weak

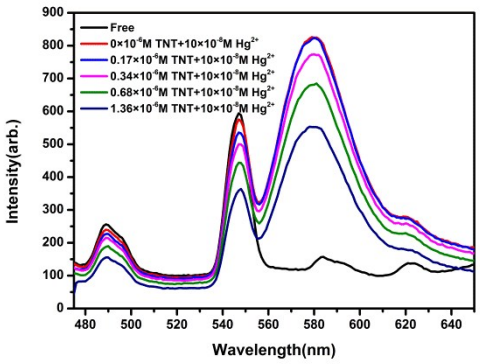

Fig.11 Emission spectra of R/Au/Tb-BTC with 10×10^{-8} M Hg^{2+} and different concentration of TNT (0-1.36×10^{-6} M) in ethanol solution, the excitation wavelength is 353 nm.

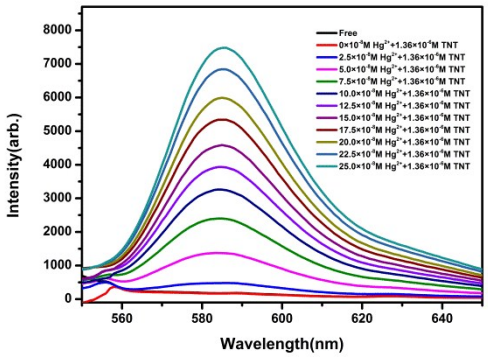

Fig.12 Fluorescence spectra of R/Au/Tb-BTC with 1.36×10^{-6} M TNT and different concentrations of Hg^{2+} (0-25×10^{-8} M) in aqueous solution when excited at 530 nm.

fluorescence intensity at 584 nm (excited at 353 nm). When adding 10×10^{-8} M of Hg^{2+} to the solution, a significant enhancement of fluorescence intensity at 584 nm was observed, which was due to the opening-Spirolactam form of rhodamine groups after addition of Hg^{2+}. In addition, the intensity of the characteristic fluorescence peak of Tb^{3+} at 550 nm slightly decreased. This change may be due to the reason that the interaction between Hg^{2+} and BTC linker diminished energy transfer efficiency from BTC to Tb^{3+} in Tb-BTC.[26] Upon addition of TNT, the intensity of the characteristic fluorescence peak of Tb^{3+} at 550 nm decreased significantly. Therefore, the prepared R/Au/Tb-BTC was able to detect TNT in ethanol solution containing Hg^{2+}.

The detection property of the R/Au/Tb-BTC for Hg^{2+} in aqueous solution containing TNT was investigated (Fig. 12). We can see that free R/Au/Tb-BTC solution showed weak fluorescence intensity at 584 nm (excited at 530 nm). There was no fluorescence enhancement when adding 1.36×10^{-6} M TNT to the solution, but upon addition of Hg^{2+}, the fluorescence intensity at 584 nm enhanced markedly. The results revealed that the R/Au/Tb-BTC could be applied to detect Hg^{2+} in aqueous solution containing TNT.

When TNT and Hg^{2+} coexist in ethanol solution, the R/Au/

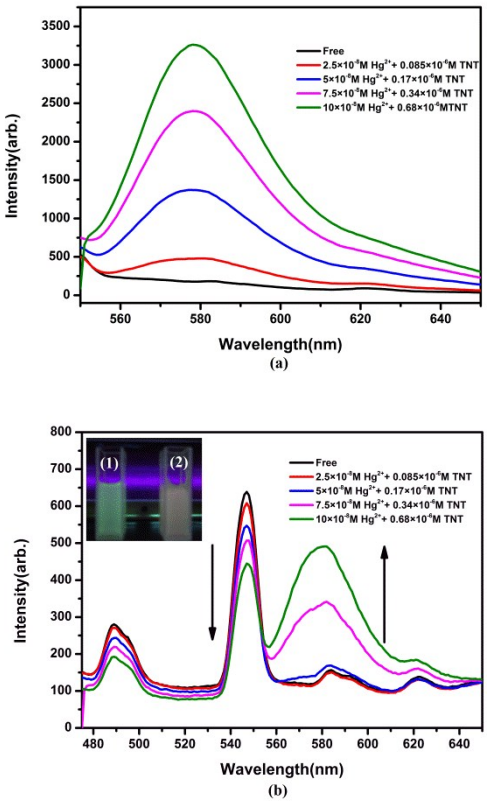

Fig.13 Fluorescence spectra of R/Au/Tb-BTC with different concentrations of Hg^{2+} (0-10×10^{-8} M) and TNT (0-0.68×10^{-6} M) in ethanol solution: (a) excited at 530 nm; (b) excited at 353 nm. Inset: the fluorescence change (1) R/Au/Tb-BTC (2) R/Au/Tb-BTC + 0.68×10^{-6} M TNT + 10×10^{-8} M Hg^{2+}.

Tb-BTC could detect them respectively. Firstly, the R/Au/Tb-BTC can be applied to detect Hg^{2+} excited at 530 nm. As shown in Fig. 13a, We can see that free R/Au/Tb-BTC solution shows weak fluorescence intensity at about 580 nm. Upon addition of Hg^{2+}, the fluorescence intensity at 580 nm enhances markedly, which has a slight blue shift compared with that in aqueous solution due to the solvent effects. Since the characteristic luminescence peaks of Tb^{3+} ions at about 584 nm can't be excited at 530 nm, the intensity of 580 nm peak can be used to analyze the concentration of Hg^{2+} in the solution. Then the chemosensor is excited at 353 nm to detect TNT, as shown in Fig. 13b. We can see that free R/Au/Tb-BTC exhibits intense fluorescence intensity at 550 nm and weak fluorescence intensity at 584 nm. When the solution was gradually added TNT and Hg^{2+} simultaneously, the intensity of the peak at 550 nm significantly weakened mainly due to the electron transfer from the Tb-BTC to the TNT. On the other hand, a significant increase of fluorescence intensity at 584 nm was observed because of the opening-Spirolactam form of rhodamine groups resulting from the complexation of mercury ions with the R. In addition, a blue shift for the fluorescence band from 584 nm to 580 nm could also be seen. Meanwhile, the fluorescence of the solution changed from green to light pink under the 254 nm UV light (Fig. 13b inset). These phenomena imply the coexistence of TNT in the solution besides Hg^{2+}.

4 Conclusions

In conclusion, a dual-functional fluorescent chemosensor R/Au/Tb-BTC for selective detection of nitroaromatic compounds and Hg^{2+} has been prepared via a simple and effective method. The chemosensor can not only sensitively detect nitroaromatic compounds in ethanol solution, especially 2,4,6-trinitrotoluene, but also sensitively detect Hg^{2+} in aqueous solution. Thus the prepared R/Au/Tb-BTC was successfully endowed with dual functionality. The sensor presents excellent anti-disturbance ability when exposed to a series of common organic chemicals or competitive cations. Furthermore, when 2,4,6-trinitrotoluene and Hg^{2+} coexist in ethanol solution, the R/Au/Tb-BTC could detect them respectively using different excitation wavelengths. These results may contribute to design more dual-functional chemosensor for detection of pollutants.

Acknowledgements

The authors acknowledge the financial support from the Program for New Century Excellent Talents in University (NCET-04-0270).

Notes and references

1 N. Venkatramaiah, S. Kumar and S. Patil, *Chem-Eur. J.*, 2012, **18**, 14745.
2 (a) J. Yinon, *Trac-Trend. Anal. Chem.,* 2002, **21**, 292; (b) S. Huang, L. Kolaitis and D. M. Lubman, *Appl. Spectrosc.*, 1987, **41**, 1371.
3 (a) S. Cheng, J. Dou, W. Wang, C. Chen, L. Hua, Q. Zhou, K. Hou, J. Li and H. Li, *Anal. Chem.*, 2013, **85**, 319; (b) M. Tabrizchi and V. Ilbeigi, *J. Hazard. Mater.*, 2010, **176**, 692.
4 (a) L. Ma, B. Xin and Y. Chen, *Analyst*, 2012, **137**, 1730; (b) N. L. Sanders, S. Kothari, G. Huang, G. Salazar and R. G. Cooks, *Anal. Chem.*, 2010, **82**, 5313.
5 (a) H. Wackerbarth, C. Salb, L. Gundrum, M. Niederkrueger, K. Christou, V. Beushausen and W. Vioel, *Appl. Optics*, 2010, **49**, 4362; (b) M. L. Lewis, I. R. Lewis and P. R. Griffiths, *Appl. Spectrosc.*, 2004, **58**, 420.
6 (a) X. Cao, S. Jing, Y. Tian, Y. Chi, X. Zhao, W. Ren, S. Qiao, D. Gu and L. Liu, *Hejishu*, 2005, **28**, 881; (b) G. Vourvopoulos and P. C. Womble, *Talanta*, 2001, **54**, 459.
7 (a) Y. Yang, Y. Li, H. Wang, T. Li and B. Wu, *Nucl. Instrum. Meth. A*, 2007, **579**, 400; (b) D. Bilcliffe, *Mater. World*, 2005, **13**, 24.
8 (a) K. Zhang, H. Zhou, Q. Mei, S. Wang, G. Guan, R. Liu, J. Zhang and Z. Zhang, *J. Am. Chem. Soc.*, 2011, **133**, 8424; (b) B. Liu, C. Tong, L. Feng, C. Wang, Y. He and C. Lue, *Chem-Eur. J.*, 2014, **20**, 2132; (c) M. Jurcic, W. J. Peveler, C. N. Savory, D. O. Scanlon, A. J. Kenyon and I. P. Parkin, *J. Mater. Chem. A*, 2015, **3**, 6351.
9 (a) M. Hirscher, B. Panella and B. Schmitz, *Micropor. Mesopor. Mat.*, 2009, **129**, 335; (b) Y. Huang and S. Ke, *Appl. Mech. Mater.*, 2013, **316-317**, 946.
10 (a) O. G. Nik, X. Chen and S. Kaliaguine, *J. Membrane Sci.*, 2012, **413-414**, 48; (b) R. Adams, C. Carson, J. Ward, R. Tannenbaum and W. Koros, *Micropor. Mesopor. Mat.*, 2010, **131**, 13.
11 (a) M. B. Lalonde, O. K. Farha, K. A. Scheidt and J. T. Hupp, *ACS Catal.*, 2012, **2**, 1550; (b) K. Leus, I. Muylaert, M.

Vandichel, G. B. Marin, M. Waroquier, S. V. Van and D. V. P. Van, *Chem. Commun.*, 2010, **46**, 5085.
12 (a) M. D. Allendorf, A. Schwartzberg, V. Stavila and A. A. Talin, *Chem-Eur. J.*, 2011, **17**, 11372; (b) O. R. Evans and W. Lin, *Chem. Mater.*, 2001, **13**, 2705.
13 (a) B. Chen, S. Xiang and G. Qian, *Accounts Chem. Res.*, 2010, **43**, 1115; (b) M. D. Allendorf, C. A. Bauer, R. K. Bhakta and R. J. T. Houk, *Chem. Soc. Rev.*, 2009, **38**, 1330.
14 (a) K. Liu, G. Jia, Y. Zheng, Y. Song, M. Yang, Y. Huang, L. Zhang and H. You, *Inorg. Chem. Commun.*, 2009, **12**, 1246; (b) B. Chen, Y. Yang, F. Zapata, G. Lin, G. Qian and E. B. Lobkovsky, *Adv. Mater.*, 2007, **19**, 1693.
15 S. Ding, W. Wang, L. Qiu, Y. Yuan, F. Peng, X. Jiang, A. Xie, Y. Shen and J. Zhu, *Mater. Lett.*, 2011, **65**, 1385.
16 H. Xu, F. Liu, Y. Cui, B. Chen and G. Qian, *Chem. Commun.*, 2011, **47**, 3153.
17 J. Xiao, L. Qiu, F. Ke, Y. Yuan, G. Xu, Y. Wang and X. Jiang, *J. Mater. Chem. A*, 2013, **1**, 8745.
18 J. Qian, L. Qiu, Y. Wang, Y. Yuan, A. Xie and Y. Shen, *Dalton T.*, 2014, **43**, 3978.
19 (a) M. Greger, Y. Wang and C. Neuschuetz, *Environ. Pollut.*, 2005, **134**, 201; (b) E. Esteban, E. Moreno, J. Penalosa, J. I. Cabrero, R. Millan and P. Zornoza, *Environ. Exp. Bot.*, 2008, **62**, 316; (c) T. W. Clarkson and L. Magos, *Crit. Rev. Toxicol.*, 2006, **36**, 609; (d) T. Syversen and P. Kaur, *J. Trace Elem. Med. Bio.*, 2012, **26**, 215.
20 (a) C. Yuan, K. Zhang, Z. Zhang and S. Wang, *Anal. Chem.*, 2012, **84**, 9792; (b) J. Hatai, S. Pal, G. P. Jose and S. Bandyopadhyay, *Inorg. Chem.*, 2012, **51**, 10129; (c) J. Bell, I. Samb, P. Y. Toullec, O. Mongin, M. Blanchard-Desce, V. Michelet and I. Leray, *New J. Chem.*, 2014, **38**, 1072.
21 (a) Y. Zhao, X. Zhang, Z. Han, L. Qiao, C. Li, L. Jian, G. Shen and R. Yu, *Anal. Chem.*, 2009, **81**, 7022; (b) S. Goswami, D. Sen, N. K. Das, H. Fun and C. K. Quah, *Chem. Commun.*, 2011, **47**, 9101.
22 (a) Q. Zou, L. Zou and H. Tian, *J. Mater. Chem.*, 2011, **21**, 14441; (b) B. Liu, Y. Chen, B. Song and Y. Liu, *Chem. Commun.*, 2011, **47**, 4418.
23 (a) N. Zhang, G. Li, Z. Cheng and X. Zuo, *J. Hazard. Mater.*, 2012, **229-230**, 404; (b) Z. Cheng, G. Li, N. Zhang and H. Liu, *Dalton T.*, 2014, **43**, 4762.
24 M. H. Lee, S. J. Lee, J. H. Jung, H. Lim and J. S. Kim, *Tetrahedron*, 2007, **63**, 12087.
25 (a) N. L. Rosi, J. Kin, M. Eddaoudi, B. Chen, M. O'Keeffe and O. M. Yaghi, *J. Am. Chem. Soc.*, 2005, **127**, 1504; (b) B. Chen, L. Wang, F. Zapata, G. Qian and E. B. Lobkovsky, *J. Am. Chem. Soc.*, 2008, **130**, 6718.
26 D. Cai, H. Guo, L. Wen and C. Liu, *CrystEngComm*, 2013, **15**, 6702.
27 Y. Xiao, L. Wang, Y. Cui, B. Chen, F. Zapata and G. Qian, *J. Alloy. Compd.*, 2009, **484**, 601.
28 (a) J. C. Sanchez, A. G. Dipasquale, A. L. Rheingold and W. C. Trogler, *Chem. Mater.*, 2007, **19**, 6459; (b) S. Doose, H. Neuweiler and M. Sauer, *ChemPhysChem*, 2009, **10**, 1389.
29 J. Yang, S. Aschemeyer, H. P. Martinez and W. C. Trogler, *Chem. Commun.*, 2010, **46**, 6804.
30 D. Wu, W. Huang, C. Duan, Z. Lin and Q. Meng, *Inorg. Chem.*, 2007, **46**, 1538.

A dual-functional fluorescent chemosensor for selectively detecting 2,4,6-trinitrotoluene and Hg^{2+} was established by immobilizing rhodamine derivative onto Tb-BTC via gold.